RESEARCH ARTICLE

PROTEINS WILEY

Crystal structure of FAD-independent methylene-tetrahydrofolate reductase from *Mycobacterium hassiacum*

Manuel Gehl[1] | Ulrike Demmer[2] | Ulrich Ermler[2] | Seigo Shima[1]

[1]Max Planck Institute for Terrestrial Microbiology, Marburg, Germany

[2]Max Planck Institute of Biophysics, Frankfurt am Main, Germany

Correspondence
Seigo Shima, Max Planck Institute for Terrestrial Microbiology, Marburg, Germany.
Email: shima@mpi-marburg.mpg.de

Abstract

FAD-independent methylene-tetrahydrofolate (methylene-H_4F) reductase (Mfr), recently identified in mycobacteria, catalyzes the reduction of methylene-H_4F to methyl-H_4F with NADH as hydride donor by a ternary complex mechanism. This biochemical reaction corresponds to that of the ubiquitous FAD-dependent methylene-H_4F reductase (MTHFR), although the latter uses a ping-pong mechanism with the prosthetic group as intermediate hydride carrier. Comparative genomics and genetic analyses indicated that Mfr is indispensable for the growth of *Mycobacterium tuberculosis*, which lacks the MTHFR encoding gene. Therefore, Mfr appears to be an excellent target for the design of antimycobacterial drugs. Here, we report the heterologous production, enzymological characterization, and the crystal structure of Mfr from the thermophilic mycobacterium *Mycobacterium hassiacum* (hMfr), which shows 78% sequence identity to Mfr from *M. tuberculosis*. Although hMfr and MTHFR have minor sequence identity and different catalytic mechanisms, their structures are highly similar, thus suggesting a divergent evolution of Mfr and MTHFR from a common ancestor. Most of the important active site residues of MTHFR are conserved and equivalently positioned in the tertiary structure of hMfr. The Glu9Gln variant of hMfr exhibits a drastic reduction of the catalytic activity, which supports the predicted function of the glutamate residue as proton donor in both hMfr and MTHFR. Thus, highly similar binding modes for the C_1-carriers and the reducing agents in hMfr and MTHFR are assumed.

KEYWORDS
crystal structure, divergent evolution, drug design, methylene-tetrahydrofolate reductase, tuberculosis

1 | INTRODUCTION

Estimated ten million people are infected with tuberculosis each year and more than one million succumb to the disease.[1] Enhanced by increasing drug resistance, tuberculosis poses an outstanding public health threat.[2] Therefore, the development of novel antimycobacterial agents is urgently needed.[3] One of the key challenges in antimicrobial drug development is the discovery of new enzyme targets that are unique to the pathogen.[4,5]

The methylene-tetrahydrofolate (methylene-H_4F) reductase (MTHFR) is a ubiquitous enzyme involved in the central carbon metabolism of eukaryotes, bacteria and most archaea. This enzyme

catalyzes the reduction of methylene-H_4F to methyl-H_4F using NAD(P)H as reducing agent.[6] MTHFR of *Escherichia coli* (eMTHFR) is a homotetramer (33 kDa per monomer) and contains FAD as prosthetic group. Catalysis proceeds via a ping-pong mechanism consisting of two half reactions. FAD is reduced by NAD(P)H in the reductive half reaction, and the generated $FADH_2$ subsequently reduces methylene-H_4F in the oxidative half reaction. Crystal structures of eMTHFR, and of *Thermus thermophilus*, *Haemophilus influenza* (PDB: 5UME), *Saccharomyces cerevisiae*, and *Homo sapiens* MTHFR have been reported.[7–10] The structure of the inactive variant of eMTHFR complexed with methyl-H_4F in combination with mutational analyses strongly contributed to establish the catalytic mechanism.[11–15]

The canonical MTHFR gene was, however, not found in the majority of mycobacterial genomes. Young et al. predicted by comparative genomic analysis and structure modeling that a gene of *Mycobacterium tuberculosis* may encode a noncanonical MTHFR.[16] Later, Sah et al. found that the enzymes encoded by *MSMEG_6596* and *MSMEG_6649* in *Mycobacterium smegmatis* are noncanonical MTHFRs that do not contain FAD or any other prosthetic group but exhibit methylene-H_4F reductase activity (Figure 1). Notably, the amino acid sequence identity of the canonical and noncanonical MTHFRs was very limited. The sequence identity is only 16%–17% and the coverage is 13%–26%. Deletion of *MSMEG_6596* from *M. smegmatis* impaired growth of the strain in the absence of methionine.[17] Recently, Yu et al. reported that the protein encoded by *Rv2172c* of *M. tuberculosis* exhibits the same properties as the noncanonical MTHFR found in *M. smegmatis*. Gene deletion experiments revealed *Rv2172c* as essential for the growth of *M. tuberculosis*.[18] Apparently, the noncanonical MTHFR is the only enzyme catalyzing the reduction of methylene-H_4F in *M. tuberculosis*. Since the noncanonical MTHFR found in mycobacteria is a new type of methylene-H_4F reductase,[17] this enzyme is referred to as **m**ethylene-tetrahydro**f**olate **r**eductase (Mfr) in this article to distinguish it from the canonical MTHFR.

Since the genes encoding Mfr are found only in mycobacteria and some related bacteria, Mfr is an excellent target enzyme for the design of antimycobacterial agents. For the design of Mfr inhibitors, a high-resolution structure of Mfr is required. Here, we present the crystal structure of Mfr from *Mycobacterium hassiacum* (hMfr). *M. hassiacum* is a thermophilic *Mycobacterium*, which is able to grow at 40–65°C.[19] The thermophilic properties of the enzymes from *M. hassiacum* are advantageous for crystallization.[20] In addition, hMfr has 78% sequence identity (query coverage 87%) with its homolog from *M. tuberculosis*. Pronounced structural similarities of the active site architecture of hMfr and eMTHFR suggest an analogous catalytic setting of the hydride transfer reaction between NADH and methylene-H_4F in hMfr and between $FADH_2$ and methylene-H_4F in eMTHFR, respectively. To test this hypothesis, we performed a mutation analysis of the functional glutamate residue of hMfr.
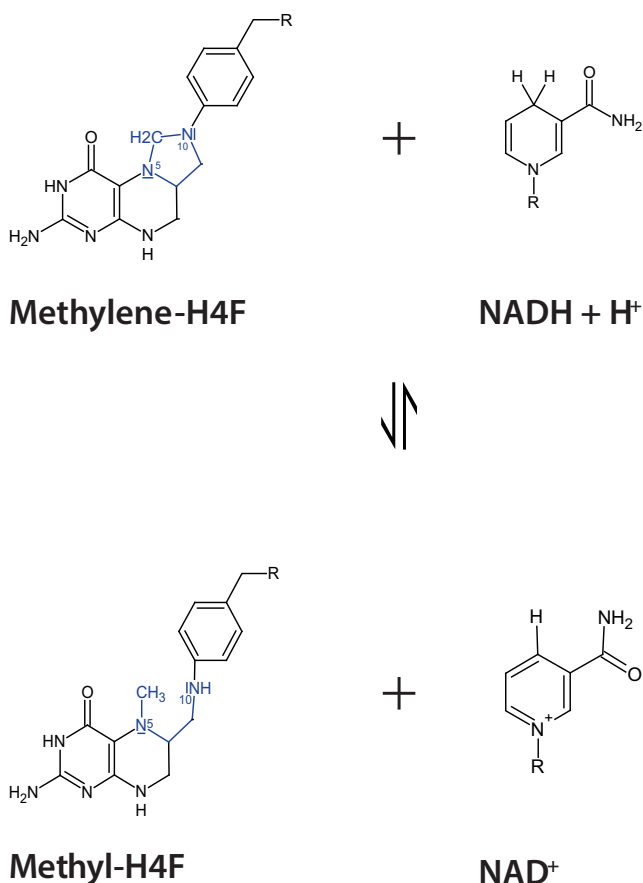
2 | RESULTS AND DISCUSSION

2.1 | Purification and characterization of hMfr

The hMfr encoding gene was codon-optimized for the expression in *E. coli*, synthesized and cloned into pET-24b(+). The heterologously over-produced protein was purified to homogeneity (Table 1 and Figure 2A). The UV-visible spectrum of hMfr revealed only one peak at 280 nm, confirming the absence of FAD (Figure 2B), as reported for Mfr from *M. smegmatis* and *M. tuberculosis*.[17,18] For crystallization, the purified enzyme fraction was further purified by size-exclusion chromatography. hMfr was eluted as a single symmetric peak at an elution volume corresponding to a molecular mass of approximately 30 kDa (Figure 2C). As the genome-deduced molecular mass of hMfr is 32 kDa, hMfr is present as a monomer. Kinetic measurements indicated that the hMfr activity is not dependent on FAD (Figure S1) in line with the findings for Mfr from *M. smegmatis* and *M. tuberculosis*.[17,18] The apparent V_{max} and K_m values of hMfr are 18 µmole min^{-1} mg^{-1} and 160 µM for methylene-H_4F and 17 µmole min^{-1} mg^{-1} and 16 µM for NADH, respectively (Table 2 and Figure S2). The biophysical and enzymatic properties of hMfr are in accordance with the previously published Mfr properties from *M. smegmatis* (see Table 2).[17] hMfr shows an optimum temperature at 70°C (Figure 3A). The thermostability of hMfr was determined by

FIGURE 1 The reaction catalyzed by hMfr. A hydride is transferred from NADH to atom C11 of methylene-H_4F that is part of the imidazolidine ring (blue). It has been postulated that a putative 5-iminium cation intermediate receives the hydride.[6]

TABLE 1 Purification of hMfr expressed in *E. coli*.

	Activity (U)	Protein (mg)	Specific activity (U/mg)	Yield (%)	Purification factor (fold)
Cell extract	1200	200	6	100	1.0
50°C heat treatment	1000	100	10	82	1.6
40% ammonium sulfate	900	86	10	73	1.7
Phenyl-sepharose HP	500	49	10	43	1.7
Resource Q	300	19	16	25	2.6

Note: The cell extract was prepared from 3 g of cells (wet mass) and the enzyme was purified aerobically as described in the materials and methods section. One unit (U) activity refers to the oxidation of 1 μmole NADH per min to form methyl-H_4F from methylene-H_4F. For kinetic analysis of the wild type and mutated hMfr, purification was performed by heat treatment and anion exchange using the Resource Q column (see Section 4). SDS-PAGE of the fraction is shown in Figure S5. The specific activity of the hMfr preparation purified by the shorter procedure was 14 ± 0.7 U/mg, which is similar to that of the preparation obtained by the longer procedure shown in this table.

FIGURE 2 Biochemical characterization of hMfr purified from recombinant *E. coli*. (A) SDS-PAGE of 2 μg purified hMfr (see also Table 1). (B) UV/Vis spectrum of purified hMfr (2.5 mg/mL) in 100 mM MOPS/NaOH pH 7.0 using a 1 cm light-path quartz cuvette. (C) Size-exclusion chromatogram of purified hMfr using a HiPrep 26/60 Sephacryl S-100 HR column. The peak at around 60 mL corresponds to hMfr.
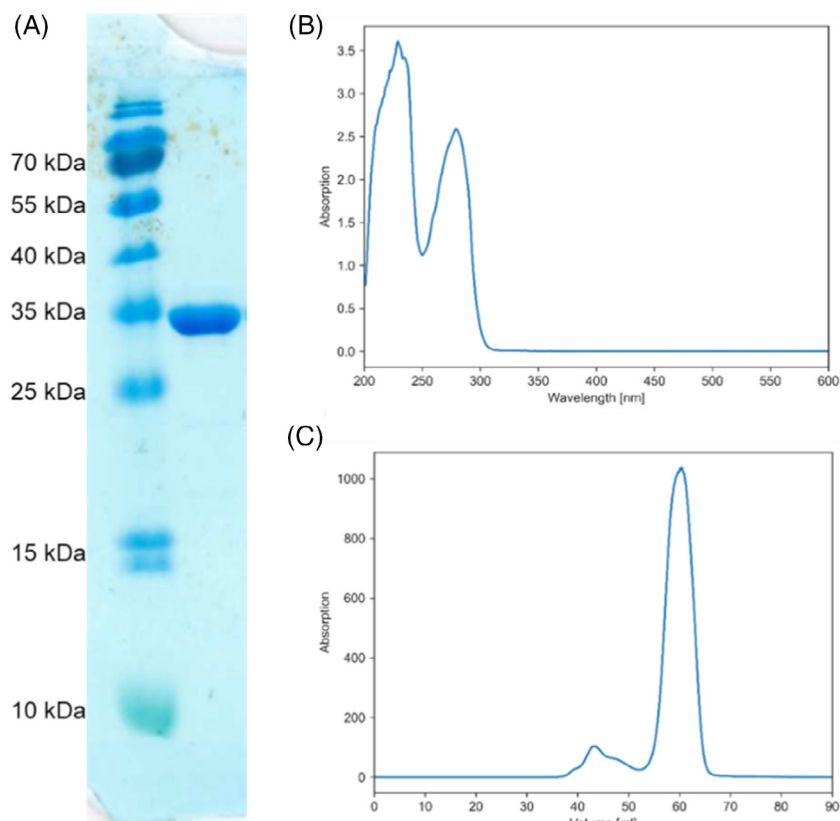
measuring the enzyme activity after incubation of the crude extract of *E. coli* for 20 min at different temperatures. We observed a slight inactivation at 60°C in the assay condition and catalytic activity was undetectable after incubation at 70°C (Figure 3B).

2.2 | Crystal structure of hMfr

Purified hMfr was crystallized by the sitting-drop vapor-diffusion method. The crystal of hMfr contained one monomer in the asymmetric unit and diffracted to 1.8 Å resolution (Table 3). The phase problem was solved by the molecular replacement method using a model structure generated by Alphafold2 as template (Figure S3). The core structure of hMfr represents an $\beta_8\alpha_8$ or triose-phosphate isomerase (TIM) barrel fold. As typically found in TIM barrel family enzymes, several prolonged segments, inserted between the secondary structure elements, play essential functional roles. In hMfr, striking insertion segments include an α-helix bundle (212–243) after β7 and two elongated loops (loop 1: 51–69 after β2 and loop 2: 118–134 after β4) that form the outer wall of a putative active site cleft (Figure 4A).

2.3 | Comparison between the structures of hMfr and eMTHFR

Both hMfr and MTHFR are TIM barrel structures (Figure 4B) with a root-mean-square deviation (RMSD) of 4.7 Å involving 240 of 296 amino acids. Despite the low sequence similarities, the insertion

TABLE 2   Kinetic properties of the hMfr wild type, hMfr_E9Q mutant, and Mfr proteins from *M. smegmatis* (MSMEG_6596 and MSMEG_6649).

Enzyme	Substrate	appK_m (µM)	appV_{max} (µmole min^{-1} mg^{-1})	appk_{cat} (min^{-1})	appk_{cat}/appK_m (min^{-1} µmole^{-1})
hMfr wild type	Methylene-H$_4$F	160 ± 62	18 ± 2.6	590 ± 85	3.9 ± 1
	NADH	16 ± 3	17 ± 0.7	540 ± 23	35 ± 5
hMfr_E9Q	Methylene-H$_4$F	250 ± 59	0.041 ± 0.004	1.3 ± 0.1	0.005 ± 0.0007
	NADH	44 ± 13	0.035 ± 0.004	1.1 ± 0.1	0.027 ± 0.054
MSMEG6596	Methylene-H$_4$F	63 ± 11	7 ± 0.3	240 ± 10	3.8 ± 1
	NADH	33 ± 8	11 ± 1	370 ± 31	11 ± 4
MSMEG6649	Methylene-H$_4$F	150 ± 30	1.2 ± 0.1	41 ± 3	0.28 ± 0.1
	NADH	110 ± 30	2.3 ± 0.3	80 ± 10	0.73 ± 0.3

Note: The data of Mfr from *M. smegmatis* was obtained from the previous publication.[17] Apparent K_m and V_{max} were measured in the presence of 300 µM methylene-H$_4$F or 100 µM NADH with the variable counter part of the substrates at 40°C. The assay was started by the addition of 10 µL of the hMfr solutions, which contained 1.9 mg/mL hMfr wild type enzyme or 150–200 mg/mL hMfr_E9Q. The standard deviations of the fitting analysis are shown. The original data of the experiments of hMfr are shown in Figure S1.
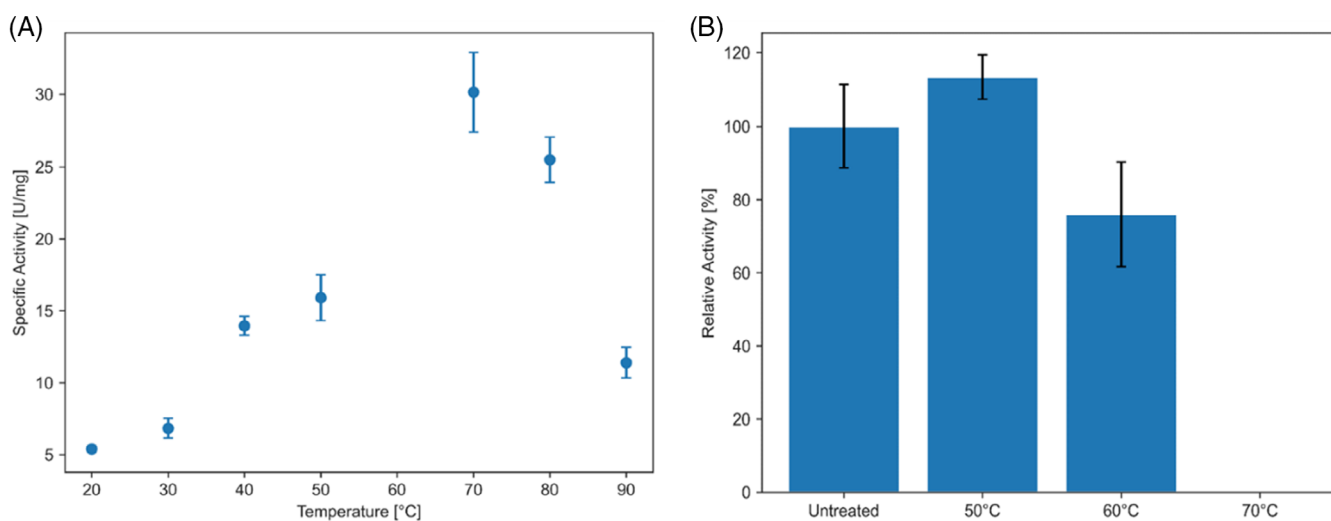
FIGURE 3   Thermophilic properties of hMfr. (A) Temperature dependency of the activity. (B) Residual activity in the cell extract after heat treatment for 20 min. Every data point consists of three independent measurements. The error bars represent the corresponding standard deviation.

regions of hMfr and eMTHFR, forming the active site cleft, are architecturally rather related (see Figure 4B). While the prolonged loop segments after β4 and β5 and those after β7 and β8 are involved in forming the putative NADH and methylene-H$_4$F binding sites, respectively, the loop segment after β2 shields the binding site of both substrates. In both eMTHFR and hMfr, the loop following β4 is partially disordered. A multiple sequence alignment of Mfr and MTHFR family members also indicates a high conservation of the insertion segments at the predicted substrate binding sites (Figure 5). Therefore, the binding modes of FAD and methyl-H$_4$F, characterized in the substrate-containing crystal structure of eMTHFR, might largely reflect the binding mode of the substrates NADH/NAD$^+$ and methylene/methyl-H$_4$F in the equivalent cleft of hMfr.

As a result, methyl-H$_4$F could be modeled directly into the potential binding site of hMfr based on the structural alignment with the crystal structures of hMfr and eMTHFR from *E. coli* containing FAD and methyl-H$_4$F (Figure 6).[10] The pterin ring of methyl-H$_4$F confidently accommodates into the predicted pocket of hMfr. The glutamate tail after the para-aminobenzoate (PABA) ring of H$_4$F interferes with the elongated segment after strand β8 (Figure 6C), which most likely changes its conformation in the hMfr-methyl-H$_4$F complex. The binding of the smaller nicotinamide ring of NADH in comparison with the larger isoalloxazine of FAD appears to be optimized by narrowing the cleft via a conformational change of loop 1 (51–69) (Figure 6C). Methylene-H$_4$F and NADH were placed into the hMfr structure by in silico molecular docking (Figure S4). Their positions and conformations approximately correspond to those taken from the aligned eMTHFR-FAD-methyl-H$_4$F-FAD structure. The distance between the hydride-donating C4 atom of NADH and the hydride-accepting C11 atom of methylene-H$_4$F in the docking model is 3.2 Å.

TABLE 3 X-ray analysis statistics.

	hMfr
Data collection	
Wavelength (Å)	1.0
Space group	$P\,4_3\,2_1\,2$
Resolution (Å)	37.32–1.8 (1.9–1.8)
Cell dimensions	
a, b, c (Å)	45.79, 45.79, 257.41
α, β, γ (°)	90, 90, 90
R_{sym} (%)[a]	9.3 (111.4)
$CC_{1/2}$[a]	0.996 (0.851)
I/σ_I[a]	9.0 (2.0)
Completeness (%)[a]	94.95 (87.48)
Redundancy[a]	4.3 (3.4)
Number of unique reflections[a]	25 392 (2248)
Refinement	
Resolution (Å)	37.31–1.8
Number of reflections	25 373
R_{work}/R_{free}[b] (%)	22.6/24.8
Number of nonhydrogen atoms	2487
Protein	2279
Ligands/ions	0
Solvent	208
Mean B-value (Å^2)	36.38
Molprobity clash score, all atoms	1.55
Ramachandran plot	
Favored regions (%)	99.65
Outlier regions (%)	0
rmsd bond lengths (Å)	0.003
rmsd bond angles (°)	0.59
PDB code	8BGR

Abbreviation: rmsd, root mean square deviation.
[a]Values relative to the highest resolution shell are within parentheses.
[b]R_{free} was calculated as the R_{work} for 5% of the reflections that were not included in the refinement.

2.4 | Possible active site residues of hMfr

Mutation experiments on eMTHFR revealed several residues crucial for the catalytic activity.[11–13,15] Glu28 is considered as a proton donor for the formation of an iminium cation intermediate, which subsequently accepts the hydride from FADH$_2$. The exchange of Glu28Gln renders the enzyme inactive and allowed the crystal structure determination of the ternary eMTHFR complex containing FAD and methyl-H$_4$F. Gln183 and Asp120 form hydrogen bonds with the pterin ring atoms N1 and N3 of methyl-H$_4$F, which are 3.1 and 2.9 Å long, respectively. Phe223 forms a π–π interaction with the PABA ring of methyl-H$_4$F in eMTHFR.

In the hMfr structure, Glu9 and Gln177 are found in the equivalent positions of Glu28 and Gln183 of eMTHFR, respectively (Figure 7). These residues are strictly conserved among Mfr and MTHFR family members (Figure 5). In the molecular docking model (Figure S4), N10 of methylene-H$_4$F is located nearby, which would allow it to interact with Glu9 via a water molecule. In the aligned sequences, the position of Asp120 of eMTHFR is replaced by Glu97 of hMfr (Figure 5). However, Glu97 is located at the beginning of α3 and points toward the solvent in the crystal structure of hMfr. Glu55 of the extended loop 1 occupies the place filled by Asp120 in eMTHFR and thereby probably stabilizes the pterin ring of methylene-H$_4$F in an analogous manner. Leu221 of hMfr is found in the equivalent position of Phe223 of eMTHFR and may stabilize the PABA ring of methylene-H$_4$F by hydrophobic interaction (Figure 7).

Based on this remarkably high structural relationship of the active site architecture of MTHFR and hMfr, we also assume a highly similar methylene/methyl-H$_4$F binding mode in MTHFR and hMfr as shown in Figures 6 and S4. To substantiate our hypothesis, we constructed an hMfr mutant, in which Glu9 was exchanged to glutamine. In eMTHFR, the corresponding Glu28Gln mutation renders the enzyme inactive. Likewise in hMfr, the catalytic activity of the Glu9Gln variant of hMfr is reduced around 400-fold compared to that of the native enzyme, while the K_m values of the substrates were only slightly changed (Table 2). This finding supported our hypothesis of a highly similar geometry between these glutamates and methyl-H$_4$F in hMfr and eMTHFR, as well as a key role for these glutamates as proton donors to form an iminium ion intermediate as described by Trimmer et al.[13] It also implicates that the hydride transfer between C4 of NADH and C11 of methylene-H$_4$F occurs at virtually the same place as the hydride transfer from the central pyrazine-ring moiety of FAD to methylene-H$_4$F in MTHFR. Thus, the active site architecture for the NADH-to-methylene-H$_4$F hydride transfer in hMfr corresponds to the reaction of the oxidative half reaction of MTHFR.

In previous studies, Mfr of *M. tuberculosis* was investigated by in vivo mutation experiments.[18] In these experiments, the Arg159Asn and Leu214Ala mutations were introduced into a *M. tuberculosis* strain.[18] Both strains showed impaired methionine biosynthesis and higher sensitivity to antifolates. Leu214 of Mfr from *M. tuberculosis* corresponds to Leu217 of hMfr, which is located next to the aforementioned Leu221 of hMfr and may play a role in interacting with the glutamate tail region of methyl H$_4$F. Arg159 from *M. tuberculosis* corresponds to Arg162 in hMfr that is located close to the ADP part of the superposed FAD on hMfr and might play a role in binding of equivalent segments of NADH in hMfr.

2.5 | Possible inhibitors of hMfr

To further investigate, the potential of Mfr as a target enzyme for the development of antimycobacterial agents, isonicotinic acid, pyrazinoic acid, and prothionamide were tested as possible inhibitors. Isonicotinic acid and pyrazinoic acid are the active forms of the first-line drugs isoniazide and pyrazinamide[23,24] while prothionamide[25] belongs to the second-line drugs against *M. tuberculosis*. These three compounds resemble NADH in their structures and their mode of action is not
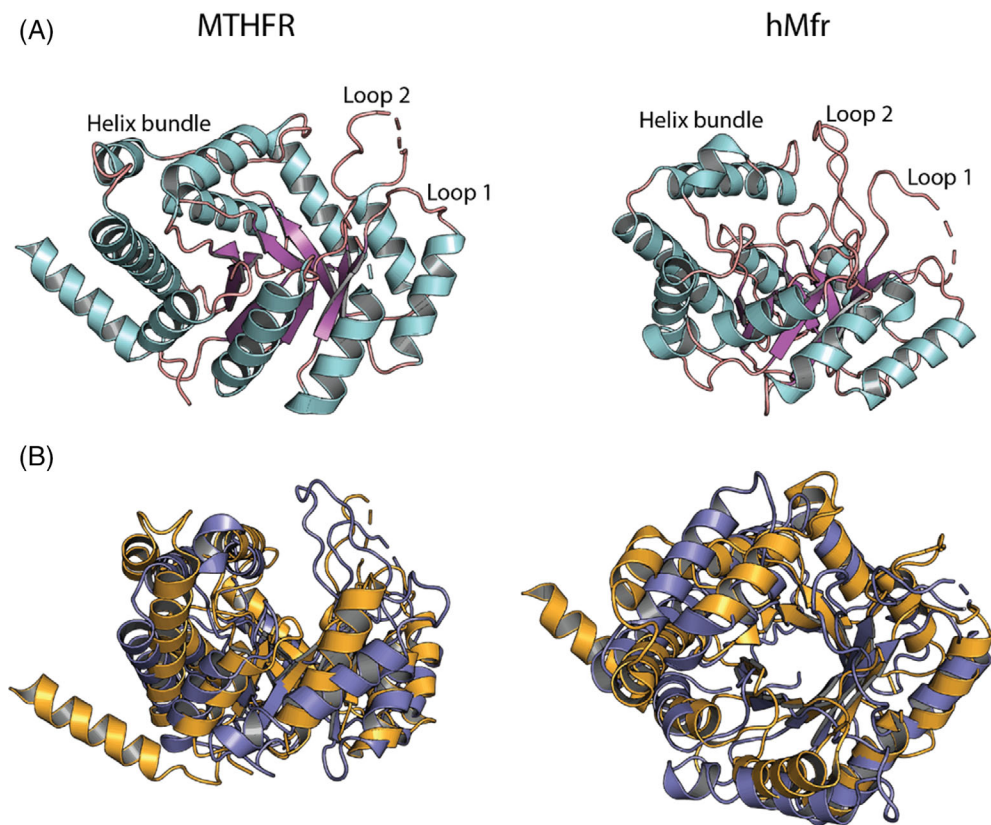
(A)

MTHFR

hMfr

(B)

FIGURE 4 Comparison of the tertiary structures of hMfr (PDB code: 8BGR) and eMTHFR (PDB code: 1ZP4).[10] (A) Cartoon representation of hMfr and eMTHFR with color-coded secondary structure elements (α-helices in cyan, β-sheets in magenta, and loops in salmon). The inserted loops and the helix bundle are labeled (see text). (B) The side and top views of the structural alignment of hMfr (blue) and eMTHFR (orange).

fully elucidated yet. Therefore, they might be potential inhibitors of Mfr. However, no inhibitory effect could be detected for any of the tested compounds (Figure 8), suggesting that this set of currently used antimycobacterial agents does not affect the Mfr reaction.

3 | CONCLUSION

The noncanonical methylene-H$_4$F reductase Mfr is a vital enzyme in mycobacteria, which includes the pathogen *M. tuberculosis*. Eukaryotic organisms including humans use instead the different FAD-containing MTHFR for the same reaction. Thus, Mfr has great potential for the design of antimycobacterial agents. We heterologously overproduced Mfr from the thermophilic mycobacterium *M. hassiacum* and characterized it as a monomeric enzyme that does not contain FAD as prosthetic group. The crystal structure of hMfr revealed a TIM barrel fold, which is also reported for the FAD-binding counterpart MTHFR. Despite the low primary structure similarity and the different enzymatic mechanism, the tertiary structures of hMfr and MTHFR did not only show the same overall fold but also highly related binding sites for methyl-H$_4$F. We mutated Glu9 of hMfr to Gln9 to mimic the Glu28Gln mutant of eMTHFR. This mutation resulted in a drastic reduction of the catalytic activity but not in a substantial loss of substrate affinity. In the assumed almost identical catalytic mechanism of MTHFR and hMfr, NADH appears to occupy the same site as FAD in eMTHFR in such a way that the hydride transfer geometry is strongly related to that of the oxidative half reaction of MTHFR. Moreover, the unexpectedly high similarities between the active sites of hMfr

and MTHFR suggest a common ancestor for both methylene-H$_4$F reductases. Taken together, the hMfr crystal structure and the deduced substrate binding mode can be applied for the development of inhibitors against Mfr.

4 | MATERIALS AND METHODS

4.1 | Construction of the vectors for overproduction of hMfr

The gene sequence of hMfr (Uniprot Accession: K5BDY6) was optimized for the codon usage of *E. coli* and synthesized by GeneScript as described below: atgaccctgaataccattgcgctggaactggtgccgccgaatagc-gatggcgccggacggtggtcgtgaacaagcggttgaggatgcgcgtaaggtgctgcgttgcgcgg cggagaccggtctggcgggtcgtatcggccacgttatgatcccgggtatgattgaggaagacccg gatcgtccgattccgatgaagccgaaaatggacgtgctggatttctggaccatcattcgtccggag ctgccgggtatccgtgtggcctgtgcacccaggttaccgcgtttctggacgaaccggcgctgcgtcgt cgtctgggtgacctgagcgcggcgggttttgatggcattgcgtttgtgggtgttccgcgtaccat-gaacgatggtgaaggtcatggtgttgcgccgaccgatgcgctgagcatgttcgcggatctggtt ccgaaccgtggcgcgatcctgattccgacccgtgacggtgaacagggccgtttcgagtttaagt gcgaacggtggtgcgacctacggcatgacccaactgctgtatagcgacgcgatcgtgggtttcct gcgtgagtttgcgcgtcgtaccgatcaccgtccggaaattctgctgagcttcggtttttgtgccga agctggaagcgaaagttggcctgatcaactggctgattcaagatccgggtaacccggcggtgg cggcggagcaagaattcgttcgtcgtctggcgggtctggagccggcggacaagcgtaaact-gatggttgatctgtacaaacgtgtgtgatcgacggtgttgcggatctgggctttccgctgagcgtg-cacctggaagcgacctatggtgttagcgtgccggccgtttgaaacctttgcggagatgctggcgt attggagcccgggtcaggggttaa.

Escherichia_coli_MTHFR

```
                                                                                                    α1
                                                                                               0000000000000
Escherichia_coli_MTHFR                       1 ...........................................MSFFHASQRDALNQSLAEVQGQI
Homo_sapiens_MTHFR                           1 MVNEARGNSSLNPCLEGSASSGSESSKDSSRCSTPGLDPERHERLREKMRRRLESGDKW.
Haemophilus_influenzae_MTHFR                 1 .......................................MSYAKEIDTLNQHIADFNKKI
Saccharomyces_cerevisiae_MTHFR               1 ...........................................MSIRDLYHAR...ASPF.
Thermus_thermophilus_MTHFR                   1 ...........................................MKIRDLLKAR...RGPL.
Mycolicibacterium_smegmatis_Mfr_MSMEG_6596   1 .............................................MGSRFVPLNT........
Mycolicibacterium_smegmatis_Mfr_MSMEG_6649   1 ...............................................MTLNT........
Mycobacterium_tuberculosis_Mfr_Rv2172c       1 ...............................................MTLNT........
Mycobacterium_hassiacum_Mfr                  1 ...............................................MTLNT........
```

Mycobacterium_hassiacum_Mfr

Escherichia_coli_MTHFR

```
              β1                            α2                     β2                    α3
             →                          0000000000           →                       0000000
Escherichia_coli_MTHFR                       24 NVSFEFFPPRT...SEMEQTLWNSIDRLSSLKPKFVSVTYGANSGERD...RTHSIIKGI
Homo_sapiens_MTHFR                           60 .FSLEFFPPRT...AEGAVNLISRFDRMAAGGPLYIDVTWHPAGDPGSDKETSSMMIAST
Haemophilus_influenzae_MTHFR                 22 NVSFEFFPPKN...EKMETLLWDSIHRLKVLKPKFVSVTYGANSGERD...RTHGIVKAI
Saccharomyces_cerevisiae_MTHFR               15 .ISLEFFPPKT...ELGTRNLMERMHRMTALDPLFITVTWGAGGTAE...KTLTLASL
Thermus_thermophilus_MTHFR                   15 .FSFEFFPPKD...PEGEEALFRTLEELKAFRPAFVSITYGAMGSTRE....RSVAWAQR
Mycolicibacterium_smegmatis_Mfr_MSMEG_6596   11 .IAELVPPNI...ERGASYAVEEAHKVLAIAAET.....GIEGRIR.....HVMIPGM
Mycolicibacterium_smegmatis_Mfr_MSMEG_6649    6 .VAELVPSNL...DLGTAHALAELQKVRKLAVDA.....GLDGRIR....HIMIPGM
Mycobacterium_tuberculosis_Mfr_Rv2172c        6 .IAELVPPNL...EGGKERAIEDARKVVQYSAAS.....GLDGRIR...HVMMPGM
Mycobacterium_hassiacum_Mfr                   6 .IAELVPPNSDGPDGGREQAVEDARKVLRCAAET.....GLAGRIG...HVMIPGM
            →                          0000000000000000
            β1                                α1                                        β2
            ▲
```

Escherichia_coli_MTHFR

```
                0000              β3          α4            β4
Escherichia_coli_MTHFR                       78 KDRTG.........LEAAPHLTCIDATPDELRTIARDYWNNGIRHIVALRGDLPPG....
Homo_sapiens_MTHFR                          116 AVNYCG........LETILHMTCCRQRLEEITGHLHKAKQLGLKNIMALRGDP.IGDQW.
Haemophilus_influenzae_MTHFR                 76 KQETG.........LEAAPHLTGIDATPEELKQIARDYWDSGIRRIVALRGDEPKG....
Saccharomyces_cerevisiae_MTHFR               67 AQQTLN........IPVCMHLTCTNTEKAIIDDALDRCYNAGIRNILALRGDPPIGEDWL
Thermus_thermophilus_MTHFR                   67 IQSLG.........LNPLAHLTVAGQSRKEVAEVLHRFVESGVENLLALRGDPPRGERVF
Mycolicibacterium_smegmatis_Mfr_MSMEG_6596   56 IDEDDDRPIEMKPKMDVLEYWNIIRPELPGLRGL.......CTQVTSFLGEEALRERLT
Mycolicibacterium_smegmatis_Mfr_MSMEG_6649   51 IEEDDGRPVEMKPKLDVLDYWELVQRELPDVRGL.......CTQVSFLGESLRRRLT
Mycobacterium_tuberculosis_Mfr_Rv2172c       51 IAEDDDRPIPMQPKLDVLDFWSIIKPELAGVHGL.......CTQVTAFMDEPSLHRRLV
Mycobacterium_hassiacum_Mfr                  54 IEEDPDRPIPMKPKMDVLDFWTIIRPELPGIRGL.......CTQVTAFLDEPALRRRLG
                                             0000000                                   0000000
                                                   α2            β3                       α3
                                                                                          ▲
```

Escherichia_coli_MTHFR

```
                             α5            β5
Escherichia_coli_MTHFR                      125 ...SGKPEM.YASDLVTLLKEV..ADFDISVAA......YPEVHPE...AKSAQA.....
Homo_sapiens_MTHFR                          166 E..EEEGGFNYAVDLVKHIRSEFGDYFDICVAG......YPKGHPE...AGSFEA.....
Haemophilus_influenzae_MTHFR                123 ..YAKKPF.YASDLVELLRSV..ADFDISVAA......YPEVHPE...AKSAQA.....
Saccharomyces_cerevisiae_MTHFR              119 DSQSNESPFKYAVDLVRYIKQSYGDKFCVGVAA......YPEGHCEGEAEGHEQDPLK..
Thermus_thermophilus_MTHFR                  118 R..PHPEGFRYAAELVALIRERYGDRVSVGGAA......YPEGHPE...SESLEA.....
Mycolicibacterium_smegmatis_Mfr_MSMEG_6596  108 A..LSGAGF.DGISFVGVPRTM.KDGEGEGVAPTDALSIYADLVPN...RGAILIPTREG
Mycolicibacterium_smegmatis_Mfr_MSMEG_6649  103 A..LIQHGF.EGIAFVGVPRTM.TDGEGAGVAPTDALSTFSHLVKH...RGVILIPTRDD
Mycobacterium_tuberculosis_Mfr_Rv2172c      103 D..LSDAGM.EGIVFVGVPRTM.QDGEGSGVAPTDALSLYRQLVAN...RGVIVIPTRDG
Mycobacterium_hassiacum_Mfr                 106 D..LSAAGF.DGIAFVGVPRTM.NDGEGHGVAPTDALSMFADLVPN...RGAILIPTRDG
                                            0..0000 →.                              0000      → ...
                                                  β4                   α4                       β5
```

Escherichia_coli_MTHFR

```
           α6          β6                 α7                β7 β8        α8
          0000000000                      0000000000000                 0000000
Escherichia_coli_MTHFR                      165 DLLNLKRKVDAGANRAITQFFFDVESYLRFRDRCV.SAGIDVEIIPGILPVSNFKQAKKF
Homo_sapiens_MTHFR                          210 DLKHLKEKVSAGADFIITQLFFEADTFFRFVKACT.DMGITCPIVPGIFPIQGYHSLRQL
Haemophilus_influenzae_MTHFR                163 DLINLKRKIDAGANHVITQFFFDIENYLRFRDRCA.SIGIDTEIVPGILPVNFKQLQKM
Saccharomyces_cerevisiae_MTHFR              171 DLVYLKEKVEAGADFVITQLFYDVEKFLTFEMLFRERISQDLPLFPGLMPINSYLLFHRA
Thermus_thermophilus_MTHFR                  162 DLRHFKAKVEAGLDFAITQLFFNNAHYFGFLERAR.RAGIGIPILPGIMPVTSYRQSAA.
Mycolicibacterium_smegmatis_Mfr_MSMEG_6596  161 EQGRFNFKCDQGATYGMTQLLYS.DAIVGFLTEFA.K...TTEHRPEILLSFGFVPKME.
Mycolicibacterium_smegmatis_Mfr_MSMEG_6649  156 ELSRFGFKCKEGATTFGMTQLLYS.DAIVNFLTEFS.R...NTDHRPEILLSFGFVPKME.
Mycobacterium_tuberculosis_Mfr_Rv2172c      156 EQGRINFKCSRGATYGMTQLLYS.DAIVGFLREFA.R...TTEHRPEILLSFGFVPKVE.
Mycobacterium_hassiacum_Mfr                 159 EQGRFEFKCERGATYGMTQLLYS.DAIVGFLREFA.R...RTDHRPEILLSFGFVPKLE.
                                            0000000000         0000000000000     0000000.0....0        →      0.
                                                  α5           β6                        α6             β7
                                                              ▲                                       ▲
```

Escherichia_coli_MTHFR

```
                          α9                   α10                     β9
             000       0000000          0000000000000000..0000000       →
Escherichia_coli_MTHFR                      224 ADMTNVRIPAWMAQMFDG...LDDDAETRKLVGANIAMD...MVKILSR.EGVKDFHFY
Homo_sapiens_MTHFR                          269 VKLSKLEVPQEIKDVIEP...IKDNDAAIRNYGIELAVS..LCQELLAS.GLVPGLHFY
Haemophilus_influenzae_MTHFR                222 ASFTNVKIPAWLVKAYDG...LDNDPTTRNLVAASVAMD...MVKILSR.EGVNDFHFY
Saccharomyces_cerevisiae_MTHFR              231 AKLSHASIPPAILSRFPPE..IQSDDNAVKSIGVDILIE..LIQEIYQRTSGRIKGFHFY
Thermus_thermophilus_MTHFR                  220 ........................SPRSAGRA...
Mycolicibacterium_smegmatis_Mfr_MSMEG_6596  215 ...AKVGLINWLIQDPGNPAVAAEQEFVSHLAEQDPAEKRRLMVDLYKRVIDGVGQLGFP
Mycolicibacterium_smegmatis_Mfr_MSMEG_6649  210 ...SEVGLIDWLIQDPDNGAVATEQQFVRRLAASEPAQKRAQMLDLYKRVIDGVITLGFP
Mycobacterium_tuberculosis_Mfr_Rv2172c      210 ...TRIGLINWLIQDPGNAAVAEQAFVQKLAGSEPARRRLMVDLYKRVLDGVADLGFP
Mycobacterium_hassiacum_Mfr                 213 ...AKVGLINWLIQDPGNPAVAAEQEFVRRLAGLEPADKRKLMVDLYKRVIDGVADLGFP
                                            00..000 00000      0000000000000000.0   0000000000000000      00000000
                                                α7        α8               α9                  α10
```

Escherichia_coli_MTHFR

```
                      α11
             0000000       000
Escherichia_coli_MTHFR                      276 TLNRAEMSYAI.......CHTLGV.RPGL.....
Homo_sapiens_MTHFR                          322 TLNREMATTEV.......LKRLGMWTEDP.....
Haemophilus_influenzae_MTHFR                274 TLNRSELTYAI.......CHMLGV.RP.......
Saccharomyces_cerevisiae_MTHFR              287 TLNLEKAIAQIVSQ............SP.....
Thermus_thermophilus_MTHFR                  228 ............................SP.....
Mycolicibacterium_smegmatis_Mfr_MSMEG_6596  272 LSVHYEVAYGVSRPAFETLAEMLEYWSPDQG....
Mycolicibacterium_smegmatis_Mfr_MSMEG_6649  267 VSLHFEAPYGVSAPAFETFAAMLDYWAPDR.....
Mycobacterium_tuberculosis_Mfr_Rv2172c      267 LSVHLEATYGVSAAAFETFAEMLAYWSPAEPGKPD
Mycobacterium_hassiacum_Mfr                 270 LSVHLEATYGVSVPAFETFAEMLAYWSPGQG....
                                                       0000000000000000
                                                 β8           α11
                                                 ▲
```
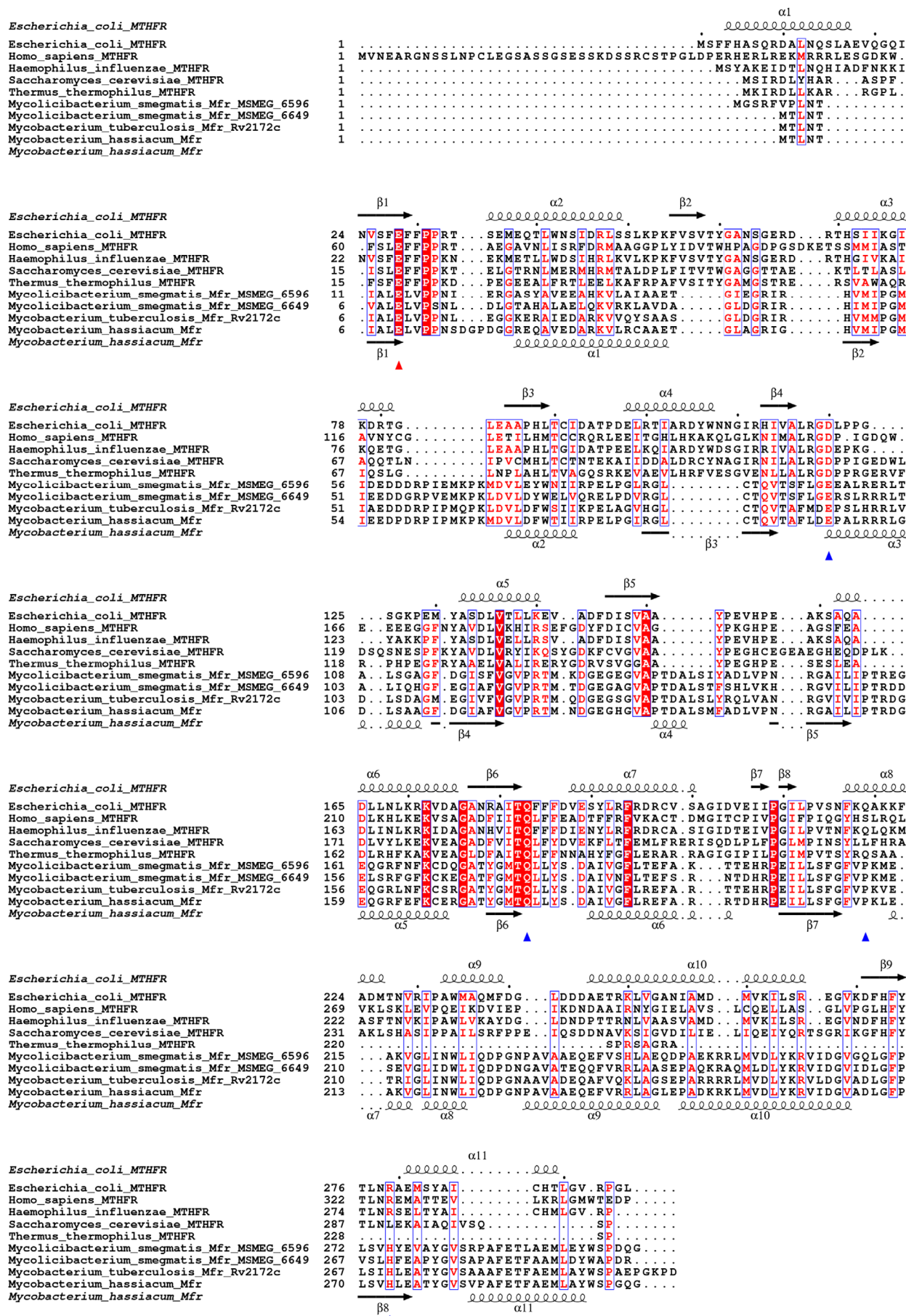
Mycobacterium_hassiacum_Mfr

FIGURE 5   Legend on next page.

The synthesized gene was cloned into pET-24b(+) between the NdeI and SalI restriction sites. The resulting plasmid pET-24b(+)_hMfr was transformed into chemically competent *E. coli* BL21(DE3) STAR cells (Thermo Fisher Scientific). The recombinant *E. coli* strain was cultivated at 37°C overnight in 100 mL of Lysogeny Broth (LB) medium as preculture. Forty milliliter of the preculture were used to inoculate two liters of prewarmed Terrific Broth (TB) medium supplemented with 50 μg/mL kanamycin sulfate in a 2 L flask (Thermo Fisher Scientific). The culture was stirred with 750 rpm and cultivated at 37°C until it reached an OD_{600} of 0.6–0.8. Then the gene expression was induced by the addition of 1 mM (final concentration) of isopropyl-β-D-1-thiogalactopyranoside (IPTG, Sigma-Aldrich). After 3 h of induction at 37°C, the cells were cooled down in an ice bath and centrifuged for 5 min at 13 000g. The cell pellets were stored at −20°C.

4.2 | Purification of hMfr

All purification steps took place under a normal aerobic environment except for the preparation of crystals. The additional size-exclusion chromatography was performed in an anaerobic chamber (Coy) filled with a N_2/H_2 (95%/5%) atmosphere. Around 3 g of cells were suspended 1:5 in 50 mM Mops/KOH pH 7.0 supplemented with 2 mM dithiothreitol (DTT, Sigma-Aldrich) and disrupted by sonication in an ice bath using a SONOPULS GM200 (Bandelin) with a KE73 tip with a 50% cycle and 160 W (2 min sonication time with 2 min pauses; in total 5 times). The cell debris were separated by centrifugation at 30000g for 30 min. To separate the thermostable hMfr from the *E. coli* proteins, the cell extract was incubated for 20 min at 50°C in a water bath and subsequently centrifuged for 20 min at 13 000g at
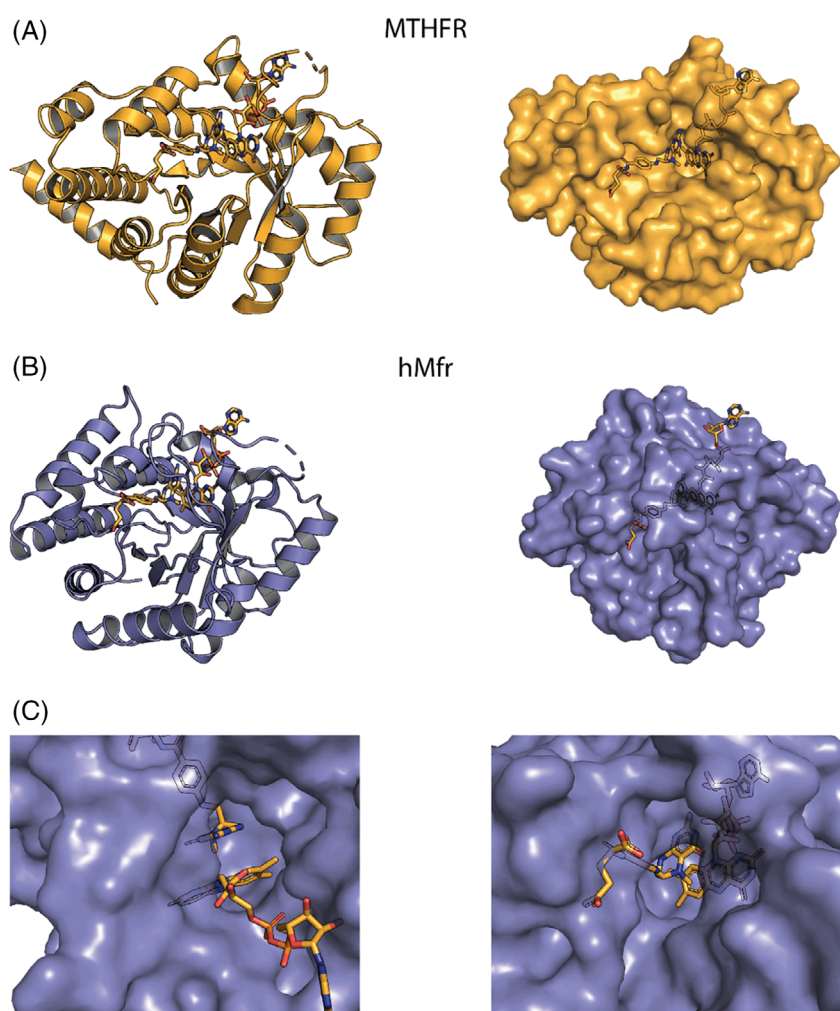
FIGURE 6 Predicted substrate binding sites of hMfr. (A) Cartoon and surface models of the complex structure of eMTHFR_E28Q (orange) in complex with methyl-H_4F and FAD (PDB code: 1ZP4). The transparency of the surface is 10%. (B) Cartoon and surface models of the structure of hMfr. Methyl-H_4F and FAD from the superimposed eMTHFR_E28Q complex are transferred and represented by orange colored carbon atoms. (C) Zoom-up views of methyl-H_4F (left panel) and FAD (right panel) models in their protein environments.

FIGURE 5 Primary structure comparison between Mfr and MTHFR. The secondary structure elements above and below the multiple sequence alignment refer to the crystal structure of eMTHFR (PDB: 1ZP4) and hMfr (PDB: 8BGR), respectively. Strictly conserved residues are depicted as white letters with red background. Residues with similar physicochemical properties are depicted as red letters in blue-lined boxes. The strictly conserved and catalytically essential glutamate residue is marked with a red triangle below the corresponding position. Residues that interact directly with methylene-H_4F via hydrogen bonds in the ternary complex structure of MTHFR are indicated by blue triangles below the corresponding position. For the sake of readability, only the catalytic domains of MTHFR from *Homo sapiens* (residues 1–343) and *Saccharomyces cerevisiae* (residues 1–302) were included. The alignment was generated using MUSCLE,[21] and the figure was created using ESPript 3.0.[22]

4°C. Ammonium sulfate (Roth) was added to the supernatant to a final saturation of 40% and the mixture was incubated under constant stirring in an ice bath for 20 min and then centrifuged for 20 min at 13 000g. The resulting supernatant was applied to two tandemly connected 5 mL HiTrap Phenyl Sepharose HP columns (Cytiva) equilibrated with 50 mM Mops/KOH pH 7.0 containing 2 mM DTT and 1.6 M ammonium sulfate. The column was washed with 1.1 M ammonium sulfate in the equilibration buffer. Elution proceeded in a single step with 0.7 M ammonium sulfate in 50 mM Mops/KOH pH 7.0 containing 2 mM DTT. The eluted protein fraction was pooled and desalted with 50 mM Mops/KOH pH 7.0 containing 2 mM DTT using a HiPrep 26/10 desalting column containing Sephadex G-25 resin. The desalted sample was applied to a 6 mL Resource Q column

equilibrated with the same buffer. Elution took place with a linear gradient from 0 to 250 mM NaCl over 15 column volumes. hMfr eluted at a conductivity between 12 and 14 mS/cm. The corresponding fractions were pooled, concentrated with an Amicon filter (10 kDa cutoff, Merck) and applied to a HiPrep 26/60 Sephacryl S-100 HR column equilibrated with 20 mM MOPS/KOH pH 7.0 containing 2 mM DTT, 150 mM NaCl and 5% (v/v) glycerol. hMfr eluted at around 60 mL retention volume. The corresponding fractions were collected and used for the preparation of anaerobic crystal plates and the measurement of the UV/vis spectrum of hMfr.

For the preparation of hMfr for enzyme assays, a shorter method was applied. After the heat treatment, the supernatant was diluted 1:1 with 50 mM Mops/KOH pH 7.0 containing 2 mM DTT and the diluted protein solution was directly applied to the Resource Q column and eluted as described above. The specific activity of the wild type hMfr purified by the shorter method was similar to that shown in Table 1 (14 ± 0.7 U/mg) and SDS-PAGE showed only minor background protein bands. The corresponding fractions were collected and used for the determination of the optimum temperature, the kinetic constants, and the inhibition assays.

FIGURE 7 Conservation of the predicted active site residues of hMfr and of eMTHFR_E28Q. The residues and methyl-H₄F derived from the crystal structure of the ternary eMTHFR_E28Q complex are shown with orange carbons and orange letters, while the residues from the hMfr apoenzyme are shown with blue carbons and blue letters.

4.3 | Enzymological assay

The activity assay of hMfr was carried out in 1 mL quartz cuvettes filled with 0.7 mL of 100 mM Mops/NaOH pH 7.0 under an N_2 atmosphere and incubated at 40°C. In the standard assay, NADH (Roth) and methylene-H₄F (Schircks Laboratories) were added to final concentrations of 100 and 300 μM, respectively. For the kinetic analysis, the concentration of NADH and methylene-H₄F was set as the standard condition and the concentration of the counter substrate was varied, as shown in Figure S1. The assay was started by the addition of 10 μL of the hMfr solutions, which contained 1.9 mg/mL wild type hMfr or 150–200 mg/mL hMfr_E9Q variant. The decrease of NADH

FIGURE 8 The effect of different antimycobacterial agents on hMfr. Every bar represents the average of three independent measurements. The error bars are the corresponding standard deviation. A final concentration of 1 mM of the respective compound was used in the assays.
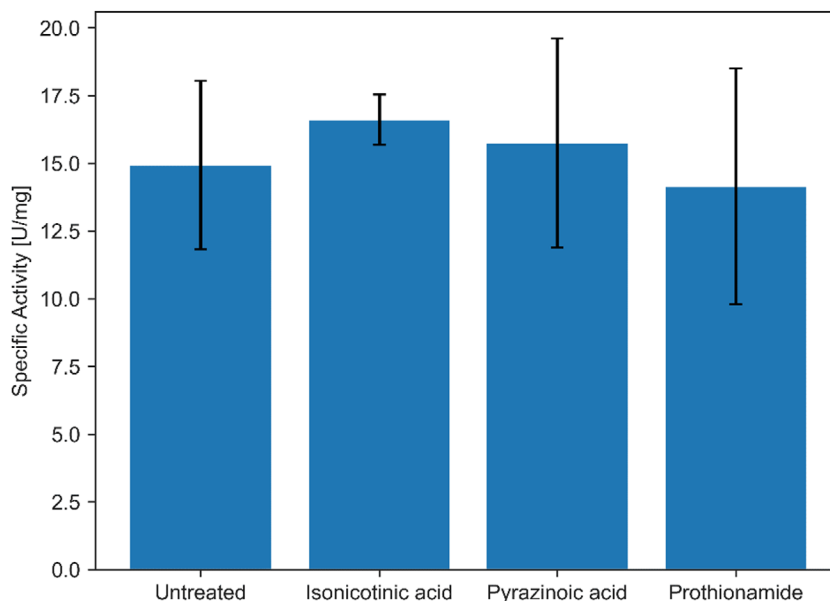
absorbance at 340 nm was measured ($\varepsilon_{340} = 6.22$ mM^{-1} cm^{-1}). For the determination of the temperature dependency, the standard conditions were used and the cuvettes were incubated at different temperatures as indicated in Figure 3. For the inhibition assays, isonicotinic acid (Sigma-Aldrich), pyrazinoic acid (Sigma-Aldrich), and prothionamide (Sigma-Aldrich) were prepared as 10 mM stock solutions in anaerobic water and were added to the enzyme assay described above to a final concentration of 1 mM.

As a negative control, we measured the activity of endogenous MTHFR from *E. coli* BL21(DE3) carrying an empty pET-24b(+) vector. The endogenous MTHFR activity was 0.5 U/mg in cell extract and 0.2 U/mg after heat treatment under the standard assay conditions described above for measuring Mfr activity. Endogenous MTHFR was only found in flow- through fractions of the Resource Q column. These experiments indicate that the purified hMfr fractions used for kinetic characterization do not contain the endogenous MTHFR activity from *E. coli*.

4.4 | Crystallization

Initially, crystallization experiments were set up at 8°C under anaerobic conditions using a N$_2$/H$_2$ (95%/5%) gas mixture to avoid oxidation of methyl-/methylene-H$_4$F. For sitting drop vapor diffusion method, 96-well screening plates (MRC 2 Well UVP, Hampton Research) were filled with 90 μL of reservoir solution and the 48-well optimization plates (MRC Maxi 48-Well Crystallization Plate (Swissci), Hampton Research) with 200 μL of reservoir solution. The crystallization plates filled with reservoir solutions were set up in the chamber 1 week prior to crystallization to make the solution anaerobic. First, crystals were found in several solutions of JB Screen Classic 1 (Jena Bioscience); for example, 25% polyethylene glycol (PEG) monomethyl ether 2000. During optimization, small rod-shaped crystals and thin plates emerged in several PEG solutions (PEG 1000–PEG 8000) in a concentration range between 10% and 30% (v/v) with no additives and no buffers. The best diffracting crystal was a thin plate, which grew in 15% (v/v) PEG 6000 with a final concentration of 30 mg/mL hMfr in the drop over the course of 4 weeks. The best crystal was transferred into the reservoir solution supplemented with 30% (v/v) glycerol and frozen.

4.5 | X-ray crystallographic analysis

The diffraction experiments were performed at 100 K on the beamline SLS X10SA (Villigen, Switzerland) equipped with a Dectris Eiger2 16 M detector. The dataset was processed with XDS and scaled with XSCALE.[26] The phase problem was solved by the molecular replacement method using PHASER[27] with an Alphafold2[28] model of hMfr. The Alphafold2 model was generated by the Colab Notebook[29] integrated into the CCP4 suite.[30] The model was built and improved in COOT[31] and refined using Phenix.refine[32] and Refmac.[33] The final model was validated using the MolProbity[34] implement of Phenix.

Data collection, refinement statistics, and PDB code for the deposited structure are listed in Table 3. The figures of the structures and the ternary complex model were generated using the PyMOL version 2.4.1 (Schrödinger) and were edited using the Adobe Illustrator.

4.6 | Kinetic data processing and figure generation

The graphs and the kinetic constants analyses were performed with Python 3.7 using Jupyter Notebook (version 6.1.4)[35] as development environment and the following packages: os, pandas,[36] seaborn,[37] matplotlib,[38] numpy,[39] and scipy.[40] The determination of the kinetic constants is based on the experimentally determined average values of the specific activity and the corresponding standard deviation from three replicates per measurement point. The Michaelis–Menten equation (vi = vmax * substrate/(km + substrate)) was used as the corresponding function for scipy.curve_fit. The resulting standard deviations for the curve fitting process were calculated from the output of the pcov parameter from scipy.cuve_fit by calculating the diagonal of the resulting array and subsequently taking the square root of the diagonal. The chemical structures from Figure 1 were generated using ChemSketch and were edited using Adobe Illustrator.

4.7 | Molecular docking of substrates

Two different docking methods were used to dock the two substrates, methylene-H$_4$F and NADH into hMfr. NADH was docked by CBDock2[41] into the Mfr-methyl-H$_4$F complex structure where the methyl-H$_4$F was transferred from the aligned eMTHFR_E28Q methyl-H$_4$F complex. Methylene-H$_4$F was docked into the Mfr structure using Autodock Vina implemented in AMDock.[42,43]

CONFLICT OF INTEREST STATEMENT

The authors declare no competing financial interest.

DATA AVAILABILITY STATEMENT

The data that support the findings of this study are available from the corresponding author upon reasonable request.

ORCID

Manuel Gehl https://orcid.org/0000-0001-5846-9539
Ulrike Demmer https://orcid.org/0000-0003-0602-8357
Ulrich Ermler https://orcid.org/0000-0001-7190-0434
Seigo Shima https://orcid.org/0000-0003-1872-8705

REFERENCES

1. Chakaya J, Khan M, Ntoumi F, et al. Global tuberculosis report 2020-reflections on the global TB burden, treatment and prevention efforts. *Int J Infect Dis*. 2021;113:S7-S12.
2. Mirzayev F, Viney K, Linh NN, et al. World Health Organization recommendations on the treatment of drug-resistant tuberculosis, 2020 update. *Eur Respir J*. 2021;57:2003300.
3. Hoagland DT, Liu JY, Lee RB, Lee RE. New agents for the treatment of drug-resistant *Mycobacterium tuberculosis*. *Adv Drug Deliver Rev*. 2016;102:55-72.
4. Stover CK, Warrener P, VanDevanter DR, et al. A small-molecule nitroimidazopyran drug candidate for the treatment of tuberculosis. *Nature*. 2000;405:962-966.
5. Pulingam T, Parumasivam T, Gazzali AM, et al. Antimicrobial resistance: prevalence, economic burden, mechanisms of resistance and strategies to overcome. *Eur J Pharm Sci*. 2022;170:106103.
6. Matthews RG. Methylenetetrahydrofolate reductase: a common human polymorphism and its biochemical implications. *Chem Rec*. 2002;2:4-12.
7. Froese DS, Kopec J, Rembeza E, et al. Structural basis for the regulation of human 5,10-methylenetetrahydrofolate reductase by phosphorylation and S-adenosylmethionine inhibition. *Nat Commun*. 2018; 9:2261.
8. Guenther BD, Sheppard CA, Tran P, Rozen R, Matthews RG, Ludwig ML. The structure and properties of methylenetetrahydrofolate reductase from *Escherichia coli* suggest how folate ameliorates human hyperhomocysteinemia. *Nat Struct Biol*. 1999;6:359-365.
9. Igari S, Ohtaki A, Yamanaka Y, et al. Properties and crystal structure of methylenetetrahydrofolate reductase from *Thermus thermophilus* HB8. *PLoS One*. 2011;6:e23716.
10. Pejchal R, Sargeant R, Ludwig ML. Structures of NADH and CH$_3$-H$_4$folate complexes of *Escherichia coli* methylenetetrahydrofolate reductase reveal a Spartan strategy for a ping-pong reaction. *Biochemistry*. 2005;44:11447-11457.
11. Lee MN, Takawira D, Nikolova AP, et al. Functional role for the conformationally mobile phenylalanine 223 in the reaction of methylenetetrahydrofolate reductase from *Escherichia coli*. *Biochemistry*. 2009; 48:7673-7685.
12. Trimmer EE, Ballou DP, Galloway LJ, Scannell SA, Brinker DR, Casas KR. Aspartate 120 of *Escherichia coli* methylenetetrahydrofolate reductase: evidence for major roles in folate binding and catalysis and a minor role in flavin reactivity. *Biochemistry*. 2005;44:6809-6822.
13. Trimmer EE, Ballou DP, Ludwig ML, Matthews RG. Folate activation and catalysis in methylenetetrahydrofolate reductase from *Escherichia coli*: roles for aspartate 120 and glutamate 28. *Biochemistry*. 2001;40:6216-6226.
14. Trimmer EE, Ballou DP, Matthews RG. Methylenetetrahydrofolate reductase from *Escherichia coli*: elucidation of the kinetic mechanism by steady-state and rapid-reaction studies. *Biochemistry*. 2001;40:6205-6215.
15. Zuo C, Jolly AL, Nikolova AP, et al. A role for glutamine 183 in the folate oxidative half-reaction of methylenetetrahydrofolate reductase from *Escherichia coli*. *Arch Biochem Biophys*. 2018;642:63-74.
16. Young DB, Comas I, de Carvalho LPS. Phylogenetic analysis of vitamin B12-related metabolism in *Mycobacterium tuberculosis*. *Front Mol Biosci*. 2015;2:6.
17. Sah S, Lahry K, Talwar C, Singh S, Varshney U. Monomeric NADH-oxidizing methylenetetrahydrofolate reductases from *Mycobacterium smegmatis* lack flavin coenzyme. *J Bacteriol*. 2020;202:e00709-e00719.
18. Yu JF, Xu JT, Yang SS, et al. Decreased methylenetetrahydrofolate reductase activity leads to increased sensitivity to para-aminosalicylic acid in *Mycobacterium tuberculosis*. *Antimicrob Agents Chemother*. 2022;66:e0146521.
19. Schröder K-H, Naumann L, Kroppenstedt RM, Reischl U. *Mycobacterium hassiacum* sp nov, a new rapidly growing thermophilic mycobacterium. *Int J Sys Bacteriol*. 1997;47:86-91.
20. Tiago I, Maranha A, Mendes V, et al. Genome sequence of *Mycobacterium hassiacum* DSM 44199, a rare source of heat-stable mycobacterial proteins. *J Bacteriol*. 2012;194:7010-7011.
21. Edgar RC. MUSCLE: multiple sequence alignment with high accuracy and high throughput. *Nucleic Acids Res*. 2004;32:1792-1797.
22. Robert X, Gouet P. Deciphering key features in protein structures with the new ENDscript server. *Nucleic Acids Res*. 2014;42:W320-W324.
23. Bendre AD, Peters PJ, Kumar J. Tuberculosis: past, present and future of the treatment and drug discovery research. *Curr Res Pharmacol Drug Discov*. 2021;2:100037.
24. Unissa AN, Subbian S, Hanna LE, Selvakumar N. Overview on mechanisms of isoniazid action and resistance in *Mycobacterium tuberculosis*. *Infect Genet Evol*. 2016;45:474-492.
25. Thee S, Garcia-Prats AJ, Donald PR, Hesseling AC, Schaaf HS. A review of the use of ethionamide and prothionamide in childhood tuberculosis. *Tuberculosis*. 2016;97:126-136.
26. Kabsch W. XDS. *Acta Crystallogr D*. 2010;66:125-132.
27. McCoy AJ, Grosse-Kunstleve RW, Adams PD, Winn MD, Storoni LC, Read RJ. Phaser crystallographic software. *J Appl Cryst*. 2007;40:658-674.
28. Jumper J, Evans R, Pritzel A, et al. Highly accurate protein structure prediction with AlphaFold. *Nature*. 2021;596:583-589.
29. Mirdita M, Schutze K, Moriwaki Y, Heo L, Ovchinnikov S, Steinegger M. ColabFold: making protein folding accessible to all. *Nat Methods*. 2022;19:679-682.
30. Winn MD, Ballard CC, Cowtan KD, et al. Overview of the CCP4 suite and current developments. *Acta Crystallogr D*. 2011;67:235-242.
31. Emsley P, Cowtan K. Coot: model-building tools for molecular graphics. *Acta Crystallogr D*. 2004;60:2126-2132.
32. Liebschner D, Afonine PV, Baker ML, et al. Macromolecular structure determination using x-rays, neutrons and electrons: recent developments in Phenix. *Acta Crystallogr D*. 2019;75:861-877.
33. Murshudov GN, Skubak P, Lebedev AA, et al. REFMAC5 for the refinement of macromolecular crystal structures. *Acta Crystallogr D*. 2011;67:355-367.
34. Williams CJ, Headd JJ, Moriarty NW, et al. MolProbity: More and better reference data for improved all-atom structure validation. *Protein Sci*. 2018;27:293-315.
35. Kluyver T, Ragan-Kelley B, Perez F, et al. Jupyter Notebooks—a publishing format for reproducible computational workflows. Positioning and Power in Academic Publishing: Players, Agents and Agendas; 2016:87-90.
36. McKinney W. Data structures for statistical computing in python. Proceedings of the 9th Python in Science Conference; 2010; Austin, TX. 51-56.

37. Waskom ML. Seaborn: statistical data visualization. *J Open Source Software*. 2021;6:3021.

38. Hunter JD. Matplotlib: a 2D graphics environment. *Comput Sci Eng*. 2007;9:90-95.

39. Harris CR, Millman KJ, van der Walt SJ, et al. Array programming with NumPy. *Nature*. 2020;585:357-362.

40. Virtanen P, Gommers R, Oliphant TE, et al. SciPy 1.0: fundamental algorithms for scientific computing in python. *Nat Methods*. 2020;17: 261-272.

41. Liu Y, Yang X, Gan J, Chen S, Xiao ZX, Cao Y. CB-Dock2: improved protein-ligand blind docking by integrating cavity detection, docking and homologous template fitting. *Nucleic Acids Res*. 2022;50:W159-W164.

42. Valdes-Tresanco MS, Valdes-Tresanco ME, Valiente PA, Moreno E. AMDock: a versatile graphical tool for assisting molecular docking with Autodock Vina and Autodock4. *Biol Direct*. 2020;15:12.

43. Trott O, Olson AJ. AutoDock Vina: improving the speed and accuracy of docking with a new scoring function, efficient optimization, and multithreading. *J Comput Chem*. 2010;31:455-461.

SUPPORTING INFORMATION

Additional supporting information can be found online in the Supporting Information section at the end of this article.